PCP
PLANT & CELL PHYSIOLOGY

Regular Paper

# Structure–Function Study of a Novel Inhibitor of Cyclin-Dependent Kinase C in Arabidopsis

Ami N. Saito[1,†], Akari E. Maeda[2,3,†], Tomoaki T. Takahara[1,†], Hiromi Matsuo[2], Michiya Nishina[3], Azusa Ono[3], Katsuhiro Shiratake[2], Michitaka Notaguchi[4], Takeshi Yanai[3,5], Toshinori Kinoshita[3,5], Eisuke Ota[1], Kazuhiro J. Fujimoto[3,5,*], Junichiro Yamaguchi[1,*] and Norihito Nakamichi[2,*]

[1]Department of Applied Chemistry, Waseda University, 513 Wasedatsurumakicho, Shinjuku, Tokyo, 162-0041 Japan
[2]Graduate School of Bioagricultural Sciences, Nagoya University, Furo-cho, Chikusa, Nagoya, 464-8601 Japan
[3]Graduate School of Science, Nagoya University, Furo-cho, Chikusa, Nagoya, 464-8602 Japan
[4]Bioscience and Biotechnology Center, Nagoya University, Furo-cho, Chikusa, Nagoya, 464-6801 Japan
[5]Institute of Transformative Bio-Molecules, Nagoya University, Furo-cho, Chikusa, Nagoya, 464-6801 Japan
[†]These authors contributed equally to this work.

*Corresponding authors: Kazuhiro J. Fujimoto, E-mail, fujimotok@chem.nagoya-u.ac.jp; Junichiro Yamaguchi, E-mail, junyamaguchi@waseda.jp; Norihito Nakamichi, E-mail, nnaka@agr.nagoya-u.ac.jp

(Received 8 July 2022; Accepted 31 August 2022)

**The circadian clock, an internal time-keeping system with a period of about 24 h, coordinates many physiological processes with the day–night cycle. We previously demonstrated that BML-259 [*N*-(5-isopropyl-2-thiazolyl) phenylacetamide], a small molecule with mammal CYCLIN DEPENDENT KINASE 5 (CDK5)/CDK2 inhibition activity, lengthens *Arabidopsis thaliana* (Arabidopsis) circadian clock periods. BML-259 inhibits Arabidopsis CDKC kinase, which phosphorylates RNA polymerase II in the general transcriptional machinery. To accelerate our understanding of the inhibitory mechanism of BML-259 on CDKC, we performed structure–function studies of BML-259 using circadian period-lengthening activity as an estimation of CDKC inhibitor activity in vivo. The presence of a thiazole ring is essential for period-lengthening activity, whereas acetamide, isopropyl and phenyl groups can be modified without effect. BML-259 analog TT-539, a known mammal CDK5 inhibitor, did not lengthen the period nor did it inhibit Pol II phosphorylation. TT-361, an analog having a thiophenyl ring instead of a phenyl ring, possesses stronger period-lengthening activity and CDKC;2 inhibitory activity than BML-259. In silico ensemble docking calculations using Arabidopsis CDKC;2 obtained by a homology modeling indicated that the different binding conformations between these molecules and CDKC;2 explain the divergent activities of TT539 and TT361.**

**Keywords:** *Arabidopsis thaliana* (Arabidopsis) • CDKC;2 • Circadian clock • In silico study • Structure–activity relationship

## Introduction

Plants coordinate photosynthesis and other metabolisms with day–night cycles in order to adapt to fluctuating environmental conditions. The circadian clock, a time-keeping system that maintains approximately 24-h period oscillations, plays an important role in this coordination (Millar 2016). The clock works in part through the integration of multiple feedback loops consisting of clock-associated genes (Nohales and Kay 2016, McClung 2019). In the model plant *Arabidopsis thaliana* (Arabidopsis), most clock-associated genes encode transcription factors, but posttranslational modifications of proteins are also important for maintaining clock function (Yan et al. 2021).

We have recently developed an approach to understanding the components of the clock and how they interact, in which small molecules were screened for perturbation of the Arabidopsis circadian clock, and their mechanisms of action were determined (Uehara et al. 2019, 2022, Nakamichi et al. 2022). This approach not only provides valuable tools for manipulating the clock, even in cases where genetic approaches fail because of genetic redundancy and the lethality by mutations of essential genes, but also uncovers posttranslational modifications essential for the clock. PHA767491 and 3,4-dibromo-7-azaindole were found to lengthen periodicity by inhibiting Casein Kinase 1 Like (CKL) family proteins (Ono et al. 2019, Uehara et al. 2019). CKL4 directly phosphorylates PSEUDO-RESPONSE REGULATOR 5 (PRR5) and TIMING OF CAB EXPRESSION 1 (TOC1, also called PRR1) protein in vitro, and therefore, inhibition of CKL activity in vivo results in upregulation of PRR5 and TOC1

*Plant Cell Physiol.* 63(11): 1720–1728 (2022) doi:https://doi.org/10.1093/pcp/pcac127, Advance Access publication on 31 August 2022, available online at https://academic.oup.com/pcp

(Uehara et al. 2019). A structure–activity relationship study of PHA767491 and its derivatives indicated that a similar molecule, AMI-331, was a potent and selective CKL inhibitor (Saito et al. 2019).

BML-259 [*N*-(5-isopropyl-2-thiazolyl) phenylacetamide], known as an animal CYCLIN DEPENDENT KINASE 5 (CDK5)/CDK2 inhibitor, lengthens the Arabidopsis clock period by inhibiting CYCLIN DEPENDENT KINASE C;2 (CDKC;2). CDKC;2 phosphorylates the RNA polymerase II C-terminal domain (Pol II CTD) (Uehara et al. 2022). In silico modeling using a human CDKC;2 homolog, CDK9, suggests that BML-259 binds to target proteins through hydrogen bonds with two nitrogen atoms and that its isopropyl group forms a CH/π bond. The binding energy and the binding state structure were used to predict binding in this case, but the binding distance between the protein and the small molecule is a new type of evaluation (Poznanski et al. 2014). The binding of small molecules to target proteins in vivo is dynamic, so it is not easily or robustly calculated by simulations using a single protein structure. Ensemble docking simulation is another in silico analysis method that takes in vivo dynamics and multiple protein conformations into consideration in the development of a binding model (Huang and Zou 2007).

In this study, we extended structure–activity relationship studies of BML-259 analogs. Strikingly, TT-539, which has the same structure as a known CDK5/CDK2 inhibitor (Helal et al. 2004) and possesses two nitrogen atoms and an isopropyl group, did not have period-lengthening activity. We also found a potent period-lengthening molecule, TT-361, which has two nitrogen atoms and the isopropyl group. Ensemble docking computational modeling using Arabidopsis CDKC;2 predicted the different binding conformations between these molecules and CDKC;2, which explains why these small molecules have different activities even though they each have two nitrogen atoms and an isopropyl group in the same locations.

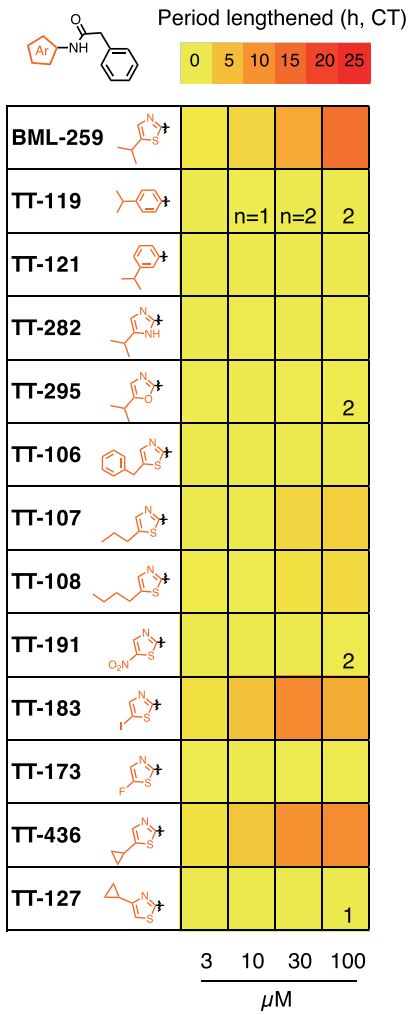


Fig. 1 Period-lengthening activity of BML-259 analogs modified at the thiazole ring positions. A heat map was generated with averaged data from three or more independent biological replicates. Data were generated from one or two biological replicates (e.g. '$n$ =1'), because of high fitting error values between a raw bioluminescence rhythm and the fitting curve (error value > 0.05, see the 'Materials and Methods' section).

## Results and Discussion

### Structure–activity relationship of BML-259

The period-lengthening activity of small molecules on the Arabidopsis circadian clock was measured via in vivo CDKC;2 inhibitory activity as a robust approach to study the structure–activity relationships of small molecule analog constituents (**Figs. 1–3**). At first, we examined whether a thiazole group is important for period-lengthening activity. Molecules with substituted phenyl, imidazole or oxazole groups replacing a thiazole have less period-lengthening activity (TT-119, TT-121, TT-282 and TT-295), suggesting that thiazole is essential for interactions with CDKC;2 and thus period-lengthening activity (**Fig. 1**). These results support our previously proposed model, which predicts that the thiazole nitrogen atom binds to the target protein (human CDK9) via a hydrogen bond (Uehara et al. 2022). The isopropyl group on the thiazole ring was next examined, and we found that isopropyl is suitable but not necessary for strong activity (**Fig. 1**). This is also consistent with our previous prediction that isopropyl binds to target proteins with CH/π bonds (Uehara et al. 2022).

With the exception of TT-258, TT-262 and TT-117, exchanging the phenylacetyl substituent for other structures diminished period-lengthening activity (TT-146, TT-170, TT-237, TT-145, TT-116 and TT-539), suggesting that phenylacetyl is an important but changeable structure (**Fig. 2**). The molecule with a substituted urea lost all period-lengthening activity (TT-539). This is intriguing because BML-259 analogs with a substituted urea group retain mammalian CDK5 and CDK2 inhibitory activities (Helal et al. 2004) (described below).

There are some variations of period-lengthening activities of molecules with phenyl group substitutions, suggesting that there are fewer restrictions on its structure (**Fig. 3**). On the whole, the structure–activity relationship study of BML-259

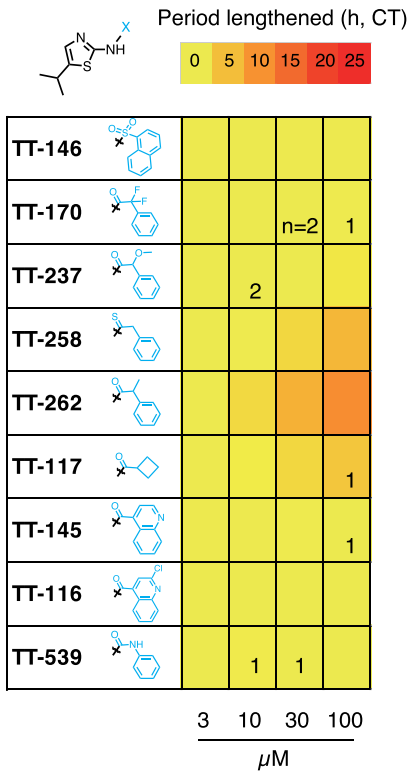


Fig. 2 Period-lengthening activity of BML-259 analogs modified at the amide-methyl ring positions. A heat map was generated with averaged data from three or more biological replicates except where indicated (i.e. '$n = 2$').

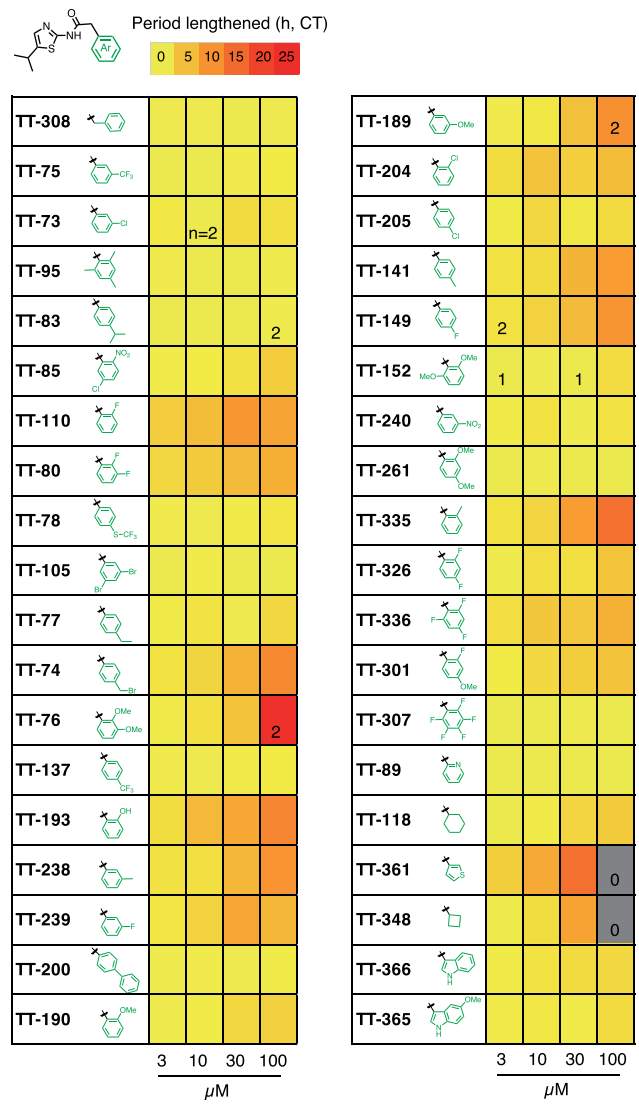


Fig. 3 Period-lengthening activity of BML-259 analogs modified at the phenyl ring positions. A heat map was generated with averaged data from three or more biological replicates except where indicated (i.e. '$n = 2$'). Gray panels indicate unidentifiable period data due to poor fitting between raw traces and the fitting curve, despite the use of four replicates.

analogs suggested that the thiazole ring and amide moieties are essential, but that the phenyl ring is less critical for maintaining period-lengthening activity.

## CDKC;2 inhibitory activity of TT-539 and TT-361

TT-539 has the same structure as an in vitro CDK5 and CDK2 inhibitor with urea in the place of the phenylacetyl group of BML-259 (Helal et al. 2004), yet it did not have period-lengthening activity in Arabidopsis (**Fig. 2**). To further understand the activity of TT-539, we analyzed the effects of TT-539 on the circadian clock in detail (**Fig. 4**). Although TT-539 treatment did not change periodicity at concentrations from 1 to 25 μM (**Fig. 4A–C**), treatment with TT-539 effectively eliminated the luminescence signal (**Fig. 4D**). Luminescence of the first circadian rhythm peak decreased with treatment in a dose-dependent manner by both BML-259 and TT-539, but the effect was much greater with TT-539 (**Fig. 4E**). To examine the decreased luminescence signal by TT-539, we measured steady-state *CCA1* messenger RNA (mRNA) levels and found that 25 μM TT-539 treatment did not reduce *CCA1* mRNA (**Supplementary Fig. S1**). Thus, TT-539 has biological activities attenuating posttranscriptional, translational and posttranslational regulations of the luciferase gene or other biological processes that eventually affect luciferase activity. BML-259 lengthens the clock period partly through the inhibition of RNA polymerase II (Pol II) by CDKC;2 (Uehara et al. 2022). Therefore, we treated Arabidopsis seedlings with TT-539 and measured the phosphorylation of Pol II. Pol II phosphorylation was no lower than the control with TT-539 treatment (**Fig. 4F**, **Supplementary Fig. S1**). TT-539 thus has no period-lengthening activity and no detectable Pol II phosphorylation inhibition activity, although it does suppress *CCA1:LUC* luminescence. This analysis supports the previously reported association between decreased Pol II phosphorylation and long periodicity (Uehara et al. 2022). It is logical to assume that BML-259 and TT-539 share target proteins other than CDKC;2, which would account for the suppression of luminescence by some as-yet-unknown mechanism.

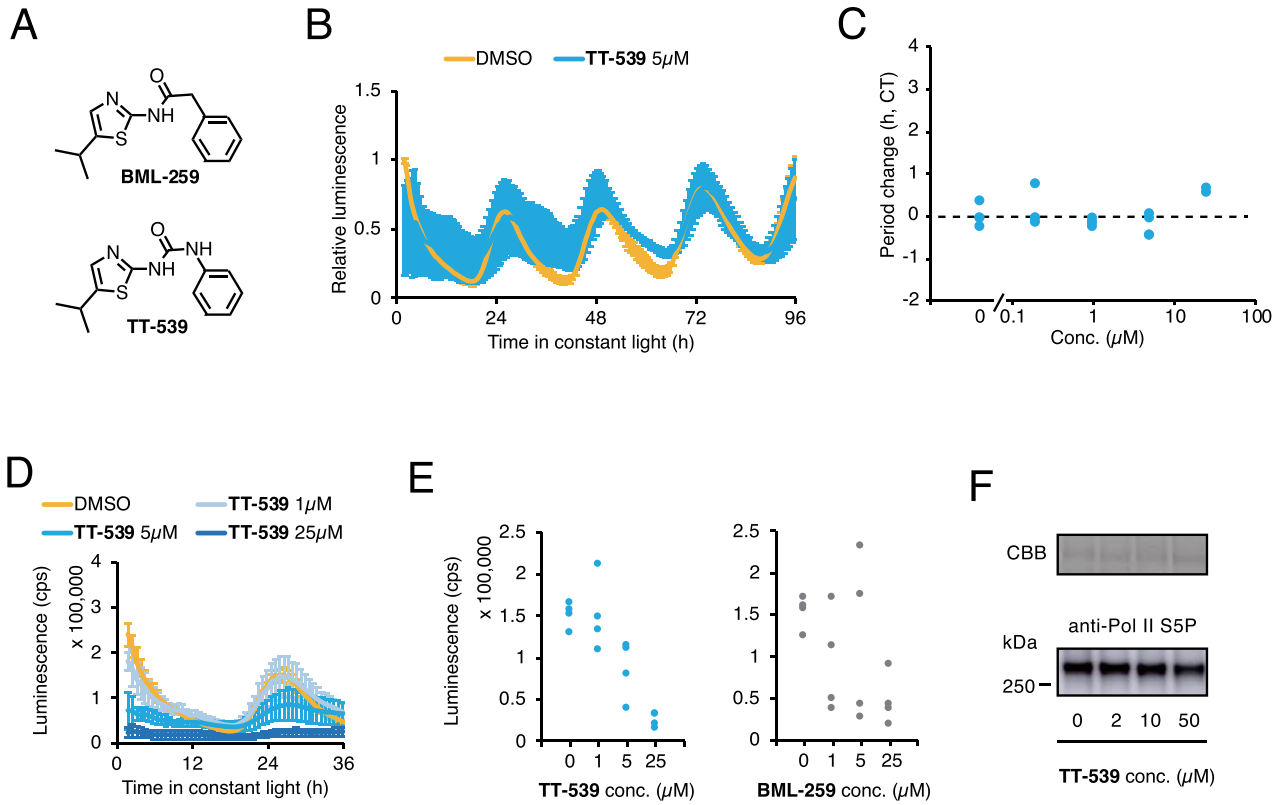


Fig. 4 TT-539 activity on the Arabidopsis clock. (A) Structures of BML-259 and TT-539. (B) Relative luminescence trace of CCA1:LUC treated with 5 μM TT-539. Error bars represent SD ($n = 4$). (C) Period alteration of CCA1:LUC seedlings treated with TT-539 ($n = 4$, except for 25 μM with two replicates due to high fitting error values between a raw bioluminescence rhythm and the fitting curve). (D, E) Luminescence of CCA1:LUC seedlings treated with TT-539 ($n = 4$). (F) Pol II CTD phosphorylation (**Supplementary Fig. S5**) in plants treated with TT-539. Similar results were obtained in replicate experiments (**Supplementary Fig. S1**).

In contrast to TT-539, some analogs have increased period-lengthening activity. For example, substituting a thiophene for the phenyl ring (TT-361) provides stronger period-lengthening activity (**Fig. 1**). TT-361 lengthened the clock period more than BML-259 did at concentrations from 1 to 25 μM (**Fig. 5B, C**). TT-361-treated Arabidopsis seedlings had lower Pol II phosphorylation than seedlings treated with BML-259, but both treatments resulted in dose-dependent phosphorylation decreases (**Fig. 5D**, **Supplementary Fig. S2A**). Kinase activity on the recombinant Pol II CTD by CDKC;2 also decreased with BML-259 and TT-361 treatment (**Fig. 5E**, **Supplementary Fig. S2B**). 1 μM BML-259 decreased the phosphorylation signal by about half of that of the untreated control. There was weak phosphorylation at 4 μM BML-259, and almost none at 10 μM. 1 μM TT-361 decreased the CTD phosphorylation signal to below half of the control level and to almost nil at 4 μM. These results suggest that CDKC;2 inhibitory activity of TT-361 is slightly stronger than that of BML-259 (**Fig. 5E**, **Supplementary Fig. S2B**).

To determine whether BML-259 and TT-361 inhibit CTD phosphorylation in evolutionarily distant plants, gramineous monocot *Brachypodium* (Poaceae) plants were grown under constant white light and temperature (22°C) conditions for 1 week and then treated with 9 μM of BML-259 or TT-361 for 1 h. Western blotting indicated that the Pol II phosphorylation signal decreased with both BML-259 and TT-361 treatment (**Fig. 5F**). Western blotting using anti-Pol II antibody–recognizing hyper- and hypophosphorylated Pol II confirmed the decreased phosphorylation of Pol II by BML-259 and TT-361, with suppression of phosphorylation signals being stronger by TT-361 than by BML-259. These results suggested that TT-361 and BML-259 can be used as CDKC inhibitors of Pol II phosphorylation in both dicots and monocots.

## In silico binding model of TT-361 and CDKC;2

Our previous study demonstrated that BML-259 binds to the ATP-binding pocket of CDK9, a mammal homolog of CDKC;2, through two hydrogen bonds and a CH/π bond (Uehara et al. 2022). The N atoms from which the hydrogen bonds are generated are conserved in both active TT-361 and inactive TT-539 molecules (**Figs. 4**, **5**) and thus presumably are the two hydrogen bonds. TT-361 and TT-539 also have isopropyl groups at the C5 position of the thiazole ring that forms a CH/π bond to CDK9 (**Figs. 4**, **5**) (Uehara et al. 2022). Therefore, the disparate CDKC;2 inhibitory activities of TT-361 and TT-539 are not simply explained by the previous binding model using mammal CDK9 as the predicted structure target of the small molecules

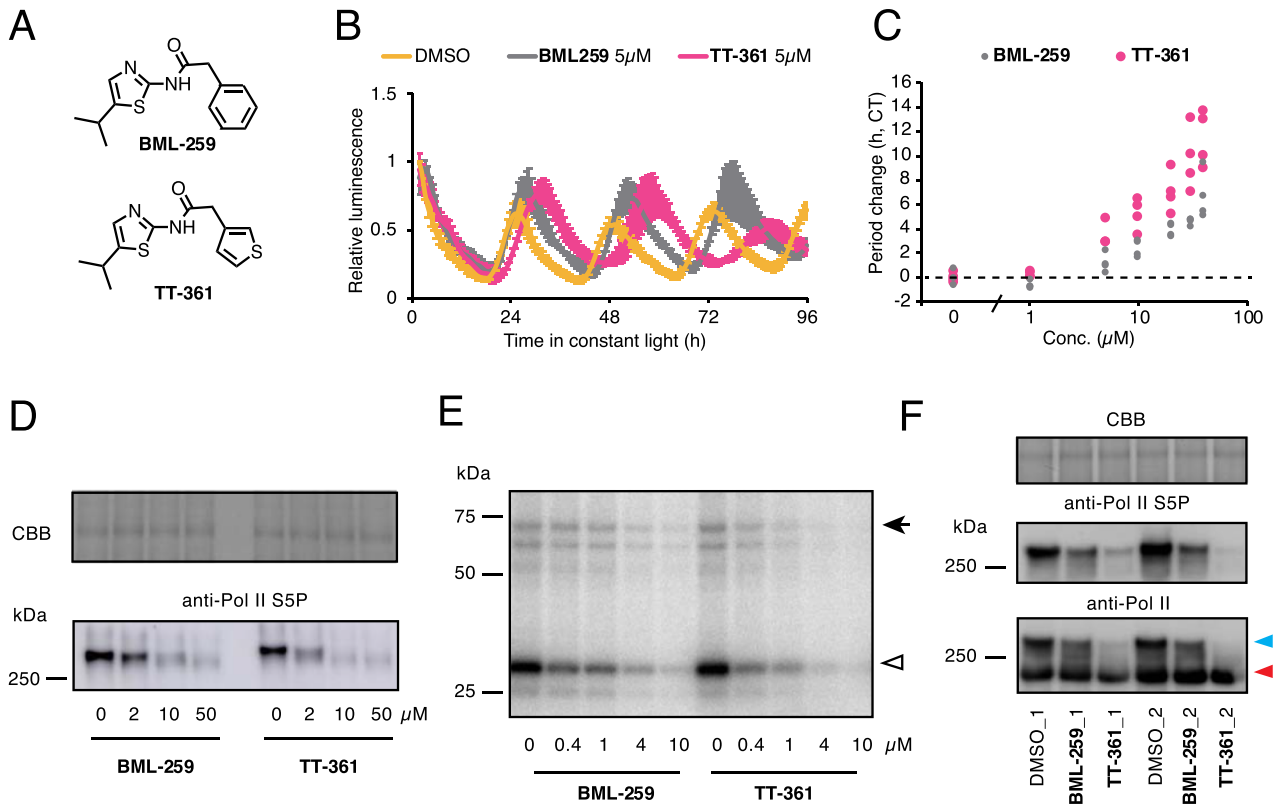


Fig. 5 TT-361 activity on the Arabidopsis clock. (A) Structures of BML-259 and TT-361. (B) CCA1:LUC traces of seedlings treated with BML-259 or TT-361 at 5 μM ($n = 4$). (C) Concentration-dependent period change of CCA1:LUC seedlings treated with BML-259 or TT-361. (D) RNA Pol II CTD phosphorylation in Arabidopsis treated with BML-259 or TT-361 ($n \geqq 3$). (E) In vitro CDKC;2 kinase activity. Arrowhead and white triangle indicate CDKC;2-FLAG and GST-CTD, respectively. (F) RNA Pol II CTD in *Brachypodium* treated with BML-259 or TT-361. Upper and lower arrows indicate phosphorylated and unphosphorylated Pol II, respectively. Similar results for (D) and (E) are shown in **Supplementary Fig. S2**.

(Uehara et al. 2022). To understand the CDKC;2 binding mechanisms of these BML-259 analogs, we performed molecular docking simulations on the predicted structure of Arabidopsis CDKC;2.

CDKC;2 is associated with its partner cyclin CYCT1;4 in vivo (Wang et al. 2014). Homology modeling with Modeller 10.1 was performed using the human CDK9-cyclinT1 complex (PDB ID: 3BLR) as the template to predict the structure of the CDKC;2-CYCT1;4 complex. When we used the full-length amino acid (a.a.) sequence of CDKC;2, some disordered or unpredictable regions were apparent in the structure. This is because specific regions of CDKC;2 do not correspond to the template CDK9. Because disordered regions are not well handled in molecular docking simulations in general, we used a 10–334 a.a. region that includes a kinase domain and is conserved in CDK9. This approach resulted in a structure with few disordered regions. Disorder regions were also found in the CYCT1;4 structure obtained with a full-length sequence of CYCT1;4, whereas the CYCT1;4 sequence from 32 to 313 a.a. yielded a structure with fewer disordered regions. The resulting constructed CDKC;2-CYCT1;4 complex was similar to that of human CDK9-cyclin T1 (**Fig. 6A**). The percentage sequence identity (%SI) between kinases and cyclins was 47.2 and 33.1, respectively. The ATP-binding pocket positions in CDKC;2 and CDK9 structurally overlap. Given that 30–50% SI to template structures means about 90% of the main chain modeled with a root-mean-square error of 1.5 Å and is suitable for docking simulation with small molecules (Baker and Sali 2001), the predicted CDKC;2-CYCT1;1 is acceptable for further in silico analyses.

Proteins can assume multiple conformations due to thermal fluctuations in solution or in vivo. To account for such protein flexibility in our model, we performed a molecular dynamics (MD) simulation using the AMBER2019 program (see the 'Materials and Methods' section). Conformational fluctuations of CDKC;2-CYCT1;4 were assessed using the root-mean-square deviation (RMSD), which gives the average displacement of the atoms relative to the reference structure in the simulation (Martinez 2015) (**Fig. 6B**). Here, we used the initial conformation of CDKC;2-CYCT1;4 as the reference structure. The simulation results showed that RMSD values were almost constant in the 50–75 ns and 75–100 ns regions, suggesting that the CDKC;2-CYCT1;4 structure was equilibrated in this time region (**Fig. 6B**). Therefore, we decided to use 51 CDKC;2-CYCT1;4 conformations from the MD trajectory in the 75–100 ns region, for the ensemble molecular docking simulations

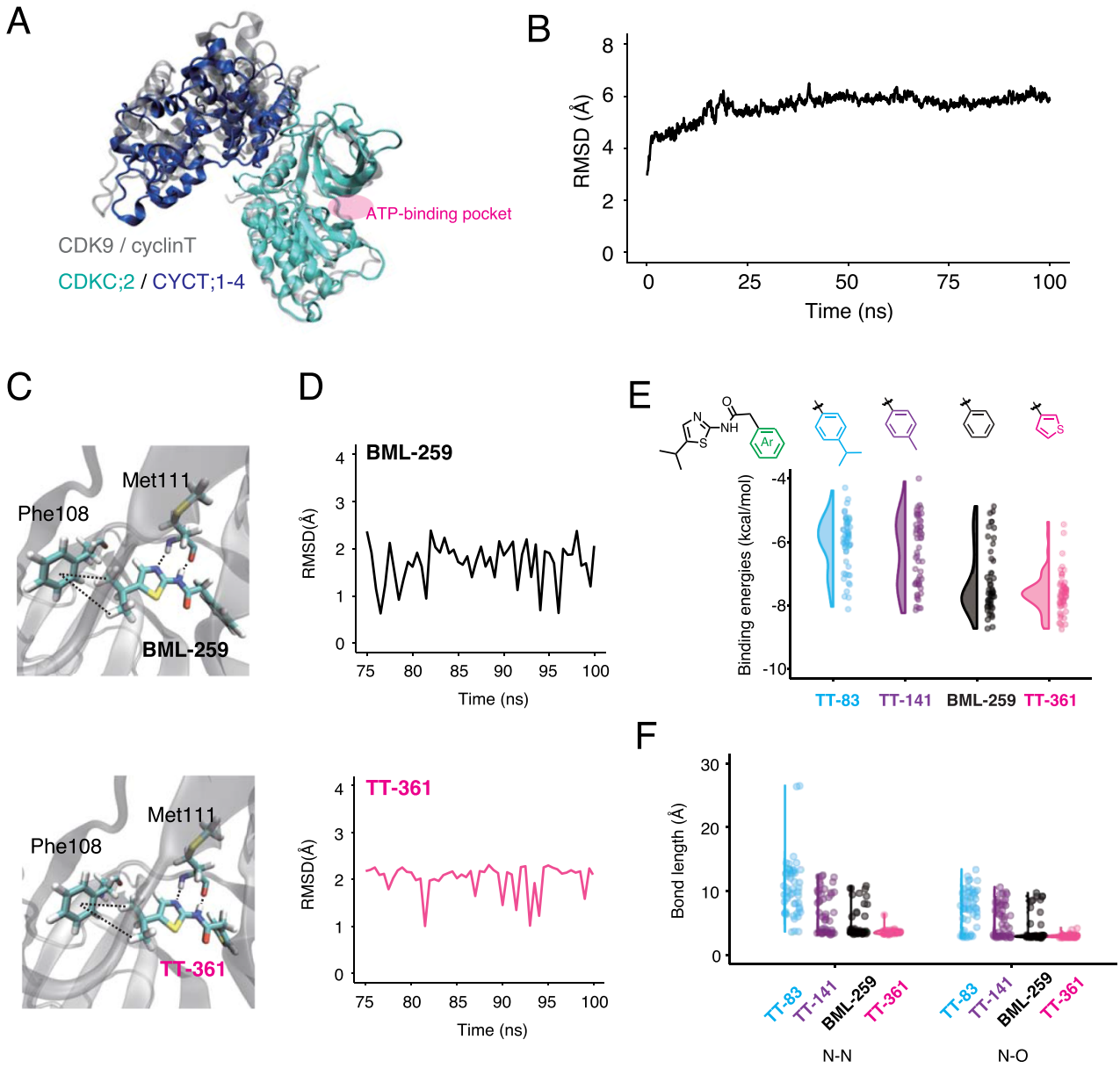


Fig. 6 In silico ensemble docking for CDKC;2 and BML-259 or TT-361. (A) Arabidopsis CDKC;2/CYCT;1–4 complex structure by a homology modeling using CDK9/cyclin T crystal (PDB ID: 3BLR). (B) Time evolution of the backbone RMSD from the initial structure along 100-ns MD trajectories for the CDKC;2/CYCT1;4 complex. (C) Predicted-binding structures of BML-259 (upper) or TT-361 (lower) with CDKC;2. Blue, yellow and red indicate nitrogen, sulfur and oxygen atoms, respectively. (D) Time evolution of the backbone RMSD from the structure of 75 ns for BML-259 (upper) and TT-361 (lower). (E) Binding energies of TT-83, TT-141, BML-259 and TT-361 with CDKC;2, as calculated by ensemble docking. (F) Distances of two hydrogen bonds between ligands and CDKC;2 Met11. N–N represents the hydrogen bond between the nitrogen of Met111 main chain and the nitrogen of ligands, and N–O represents the hydrogen bond between the oxygen of Met111 and the nitrogen of the ligands.

with BML-259 and TT-361. The results of this analysis showed that TT-361 could bind to CDKC;2 more stably than BML-259 (**Fig. 6C, D**). Average binding energies of BML-259 and TT-361 with CDKC;2 were predicted to be $-7.26 \pm 1.03$ and $-7.60 \pm 0.65$ kcal mol$^{-1}$, respectively (**Fig. 6E**), indicating that TT-361 binds more strongly to CDKC;2 than BML-259.

To understand the mechanism of strong TT-361 activity against CDKC;2, we measured the distances of hydrogen bonds and CH/π bonds between TT-361 and CDKC;2, because the activity of small molecules often correlates with their bond distances from their binding targets (Poznanski et al. 2014). A previous study suggested that the main chain of Cys106 in CDK9, which is the hinge region in the ATP-binding pocket, forms two hydrogen bonds with BML-259, and Phe103 forms a CH/π bond with BML-259 (Uehara et al. 2022). Docking simulations for the modeled CDKC;2 showed that the main chain

of Met111 in CDKC;2 can form two hydrogen bonds with both BML-259 and TT-361 (**Fig. 6C**). Phe108 in CDKC;2 can form CH/π bonds with BML-259 and TT-361. The average lengths of hydrogen bonds between the nitrogen atom of the thiazole as a ligand and CDKC;2 (a nitrogen atom in the main chain of Met111) (N–N bond) were calculated to be $4.90 \pm 2.40$ Å for BML-259 and $3.65 \pm 0.44$ Å for TT-361 as ligands. The average lengths of hydrogen bonds between the nitrogen atom of the amide as the ligand and CDKC;2 (an oxygen atom in the main chain of Met111) (N–O) are $4.03 \pm 2.20$ Å for BML-259 and $3.02 \pm 0.26$ Å for TT-361 (**Fig. 6F**). There are two possible CH/π bonds between CDKC;2 and ligands. The average lengths of one CH/π bond between the ligand and CDKC;2 were $6.23 \pm 5.06$ Å for BML-259 and $4.33 \pm 0.63$ Å for TT-361 (**Supplementary Fig. S3**). The other possible CH/π bond was $6.26 \pm 2.78$ Å for BML-259 and $5.37 \pm 0.75$ Å for TT-361. These results suggest that the shorter the hydrogen and CH/π bond lengths, the stronger the binding to CDKC;2.

Predictions of CDKC;2/BML-259 and CDKC;2/TT-361 binding implied that the moiety size at the phenyl position of BML-259 strongly affects the binding conformation. To investigate this effect, an ensemble docking simulation was also conducted with TT-141 and TT-83, which have bulkier methyl and isopropyl functional groups at the phenyl position than BML-259, with TT-141 being active and TT-83 being inactive (**Fig. 3**). The binding affinities of CDKC;2/TT-83 and CDKC;2/TT-141 were lower than those of CDKC;2/BML-259 (**Fig. 6E**). The hydrogen bond lengths between TT-141 and CDKC;2 were $6.60 \pm 3.23$ Å for N–N and $5.33 \pm 2.55$ Å for N–O (**Fig. 6F**), and for TT-83 and CDKC2, they were $10.55 \pm 4.49$ Å for N–N and $7.17 \pm 3.10$ Å for N–O (**Fig. 6F**). These results indicate that the active ligand TT-141 has shorter N–N and N–O distances than the inactive TT-83. However, the distances for TT-141 were longer than those for BML-259 and TT-361, confirming the model's assumption that the bond length, or distance, is inversely correlated with activity. These results also solidify the assumption that the size of the phenyl moiety significantly contributes to its binding affinity (**Fig. 6**).

To further validate the binding conformational model of TT-361 to CDKC;2, ensemble molecular docking simulations were performed using TT-539, an inactive molecule (**Supplementary Fig. S4**). This simulation showed that the average binding energy between TT-539 and CDKC;2 was $-6.82 \pm 0.92$ kcal $mol^{-1}$. The average lengths of the N–N and the N–O hydrogen bonds were calculated to be $5.16 \pm 2.73$ and $4.51 \pm 2.35$ Å, respectively. Although the difference in the N–N and the N–O hydrogen bond lengths between inactive TT-539 and active BML-259 and TT-361 was similar, we found that time evolution of the binding conformation of TT-539/CDKC;2 and those of BML-259/CDKC;2 and TT-361/CDKC;2 were different (**Supplementary Fig. S4**). BML-259 and TT-361 stably bound to the ATP-binding pocket in CDKC;2 from 90 to 100 ns in the simulation, whereas TT-539 rolled over in the pocket. These results indicate that there is weak binding of TT-539 to CDKC;2, which would explain the inactivity of TT-539 for inhibition of CDKC;2 (**Supplementary Fig. S4**).

We further tested the binding model of TT-361 to CDKC;2 with two ligand pairs in which one molecule is active and the other is inactive despite the fact that structures of ligands in a pair were very similar (**Supplementary Fig. S5**). Note that the simulation results with molecules possessing quite different structures may cause misinterpretation. TT-436 and TT-127 have cyclopropyl groups at C5 and C4 of the thiazolyl ring; TT-436 lengthens the clock period, whereas TT-127 does not (**Fig. 1**). The hydrogen bond distances of N–N and N–O between TT-436 and CDKC;2 were $3.57 \pm 0.22$ and $3.03 \pm 0.45$ Å, respectively (**Supplementary Fig. S5A**), and those between N–N and N–O and TT-127 and CDKC;2 were $6.83 \pm 1.48$ and $4.61 \pm 2.24$ Å, respectively. Similar analyses were performed for TT-262 and TT-237, which have 2-methyl and 2-methoxy groups, respectively; TT-262 is active, whereas TT-237 is not (**Fig. 2**). The hydrogen bond distances of N–N and N–O between TT-262 and CDKC;2 were $5.35 \pm 2.81$ and $4.85 \pm 2.59$ Å, respectively (**Supplementary Fig. S5B**). The hydrogen bond distances of N–N and N–O between TT-237 and CDKC2 were $8.67 \pm 1.86$ and $7.66 \pm 1.31$ Å, respectively. These results further validated the prediction that shorter bond lengths between N–N and N–O lead to strong CDKC;2 binding, and thus inhibition, and the converse assumption that longer bond lengths result in low or no inhibition of CDKC;2. In summary, the ensemble docking simulations with each of the ligand pairs strongly supported the conformational model of TT-361 binding with CDKC2.

## Conclusion

In this study, we performed structure–activity relationship studies of BML-259 analogs and found a strong CDKC inhibitor, TT-361. Two independent in vivo analyses estimating the activity of CDKC, circadian rhythm and Pol II phosphorylation, as well as in vitro CDKC;2 kinase assays, showed that TT-361 had stronger CDKC inhibitory activity than the parent molecule BML259. The previous binding model using human CDK9 and BML-259 failed to explain the strong activity of TT-361, nor the inactivity of TT-539. In this study, we used a CDKC;2 structure created by homology modeling and evaluated the binding energies with ensemble dockings, enabling the estimation of energies with a statistical approach. Hydrogen bond lengths and the establishment of CH/π bonds suspected to be important for binding between ligands and CDKC;2 were also evaluated with ensemble dockings. The resulting model, in which TT-361 binds to CDKC;2 more strongly than BML-259, was further supported by analyses using other pairs of BML-259 analogs. The model developed in this study and the identification of biologically active small molecules that affect the circadian clock ability to maintain its rhythm are expected to be useful for future studies of plant chemical biology.

## Materials and Methods

### Plant materials and growth conditions

Arabidopsis Columbia-0 (Col-0) accession was used as wild-type plants. *CCA1:LUC* (Nakamichi et al. 2005) and *cdkc;2 CDKC;2pro:CDKC;2-FLAG* mutants were previously reported (Uehara et al. 2022). Plants were grown on a half-strength Murashige–Skoog (MS) medium containing 2% sucrose and 0.3% gellan gum under 12-h white light (70 μmol $s^{-1}$ $m^{-2}$)/12-h dark conditions.

### Circadian rhythm and kinase assays

*CCA1:LUC* luminescence activity following small molecule treatment was measured by auto-luminescence detection (CL96, Churitsu), as previously reported (Uehara et al. 2019). In vitro CDKC;2 kinase assays were performed as previously described (Uehara et al., 2022).

### Synthesis of BML-259 analogs

Syntheses of BML-259 analogs are described in the **Supplementary material**.

### Pol II phosphorylation assay

Detection of Pol II phosphorylation in Arabidopsis seedlings with anti-Pol II CTD phospho-Ser5 antibody (MABI0603, Fujifilm Wako, Osaka, Japan) was previously described (Uehara et al. 2022). To detect Pol II phosphorylation in *Brachypodium distachyon* (*Brachypodium*), plants were grown under constant light conditions at 22°C for 1 week, divided into 5-$mm^2$ pieces with a razor blade, soaked in MS medium containing one of the small molecules and vacuum infiltrated for 30 s. Samples were kept under light for 1 h and then flash-frozen in a 2.0-ml tube with liquid nitrogen. Frozen samples were crushed with zirconia beads (ZB-50, Tomy) using a TissueLyser II (Qiagen, Venlo, Netherland), and the fine-powdered samples were dissolved in urea buffer (7.2 M urea, 50 mM Tris-HCl pH 6.8, 1% sodium dodecyl sulfate, 5% 2-mercaptoethanol) (Mizoi et al. 2019). Samples were then boiled at 95°C for 5 min and centrifuged at 14,000 g for 10 min at room temperature. Supernatants were separated by polyacrylamide electrophoresis for western blots with anti-Pol II antibody (MABI0601, Fujifilm Wako), as previously described (Uehara et al. 2022).

### In vitro CDCK;2 kinase assay

In vitro CDKC;2 kinase assay using CDKC;2-FLAG protein purified from *cdkc;2 CDKC;2pro:CDKC;2-FLAG* was conducted, as previously reported (Uehara et al. 2022).

### Gene expression analysis

Four-day-old seedling was transferred into a well of a 96-well plate with a dropper, and seedlings were treated with one-half of MS liquid containing 2% sucrose and 25 μM TT-539. As a control experiment, one-half of MS liquid containing 2% sucrose and dimethyl sulfoxide (solvent for TT-539) was used. The seedlings were cultured under 12-h light/12-h dark conditions for 1 week and flash-frozen with liquid nitrogen at 1 h after light-on. RNA extraction, reverse transcription and quantitative PCR were conducted, as previously demonstrated (Kamioka et al. 2016).

### In silico analyses

Homology modeling of Arabidopsis CDKC;2/CYCT1;4 was conducted by Modeller 10.1 (Webb and Sali 2016) with default settings, using the human CDK9/cyclin T1 complex (PDB ID: 3BLR) as a template. The N-terminal 10 a.a. and C-terminal 179 a.a. of CDKC;2 were omitted from the analysis, because there were no human CDK9 structures corresponding to these regions. Similarly, the N-terminal 32 a.a. and C-terminal 228 a.a. of CYCT1;4 were also deleted for the analysis. The truncated CDKC;2/CYCT1;4 was used for 100-ns MD simulation in the AMBER2019 program package (Case et al. 2019) with a time step of 2 fs under NPT conditions at 300 K and 1 atm, as previously demonstrated (Uehara et al. 2022). A periodic boundary box (104 × 99 × 95 $Å^3$) for MD simulation was composed of CDKC;2/CYCT1;4 and water molecules. A RMSD calculation for CDKC;2/CYCT1;4 was performed using rmsd 1.4 (https://pypi.org/project/rmsd/). The structures of BML-259 and its analogs were optimized by density functional theory at the B3LYP/6-31G* level in the Gaussian16 program package (Frisch et al. 2019), and atomic charges of the ligands were derived from the electrostatic potential fitting (Fujimoto et al. 2018). The energy score was evaluated using Schrödinger software suite Glide. RMSDs for ligands in CDKC;2 were obtained as previously described (https://github.com/charnley/rmsd). Lengths of hydrogen bonds and CH/π bonds were manually calculated in the ligand–CDKC;2 complex (51 poses from 75 to 100 ns). Graphs were generated using R 4.2.0 (R Core Team 2022).

## Supplementary Data

**Supplementary data** and note are available at *PCP* online.

## Data Availability

The data underlying this article will be shared upon reasonable request to the corresponding author.

## Funding

Japan Society for the Promotion of Science (20K21272 and 21H05656 to N.N.); Science Research on Innovative Areas (18H04428 to J.Y., 20H05411 to N.N.); Takeda Science Foundation (to N.N); World Premier International Research Center Initiative, Japan; Graduate Program of Transformative Chem-Bio Research, and Nagoya University Interdisciplinary Frontier Fellowship supported by JST and Nagoya University (to A.E.M).

## Acknowledgements

We thank Dr. Keiichi Mochida for *B. distachyon* seeds and for instructions about how to grow and handle these plants and Dr. Masaki Ito for discussion about plant CDK.

## Author Contributions

J.Y. and N.N. designed the research plan; A.N.S., T.T., E.O. and J.Y. synthesized small molecules; H.M., A.O., K.S., M.No., T.K. and N.N. performed the experiments and analyzed data; A.E.M., M.Ni., T.Y. and K.J.F. perform in silico analyses and K.J.F., J.Y. and N.N. wrote the paper.

## Disclosures

The authors have no conflicts of interest to declare.

## References

Baker, D. and Sali, A. (2001) Protein structure prediction and structural genomics. *Science* 294: 93–96.

Case, D.A., Walker, R.C., Cheatham III, T.E., Simmerling, C., Roitberg, A., Merz, K.M., et al. (2019) Amber 2019. University of California, San Francisco, CA.

Frisch, M.J., Trucks, G.W., Schlegel, H.B., Scuseria, G.E., Robb, M.A., Cheeseman, J.R., et al. (2019) Gaussian 16, Revision C.01. Gaussian, Inc., Wallingford CT.

Fujimoto, K.J., Nema, D., Ninomiya, M., Koketsu, M., Sadanari, H., Takemoto, M., et al. (2018) An in silico-designed flavone derivative, 6-fluoro-4′-hydroxy-3′, 5′-dimetoxyflavone, has a greater anti-human cytomegalovirus effect than ganciclovir in infected cells. *Antivir. Res.* 154: 10–16.

Helal, C.J., Sanner, M.A., Cooper, C.B., Gant, T., Adam, M., Lucas, J.C., et al. (2004) Discovery and SAR of 2-aminothiazole inhibitors of cyclin-dependent kinase 5/p25 as a potential treatment for Alzheimer's disease. *Bioorg. Med. Chem. Lett.* 14: 5521–5525.

Huang, S.Y. and Zou, X.Q. (2007) Ensemble docking of multiple protein structures: considering protein structural variations in molecular docking. *Proteins Struct. Funct. Genet.* 66: 399–421.

Kamioka, M., Takao, S., Suzuki, T., Taki, K., Higashiyama, T., Kinoshita, T., et al. (2016) Direct repression of evening genes by CIRCADIAN CLOCK-ASSOCIATED1 in the Arabidopsis circadian clock. *Plant Cell* 28: 696–711.

Martinez, L. (2015) Automatic identification of mobile and rigid substructures in molecular dynamics simulations and fractional structural fluctuation analysis. *PLOS One* 10: e0119264.

McClung, C.R. (2019) The plant circadian oscillator. *Biology (Basel)* 8: biology8010014.

Millar, A.J. (2016) The intracellular dynamics of circadian clocks reach for the light of ecology and evolution. *Annu. Rev. Plant Biol.* 67: 595–618.

Mizoi, J., Kanazawa, N., Kidokoro, S., Takahashi, F., Qin, F., Morimoto, K., et al. (2019) Heat-induced inhibition of phosphorylation of the stress-protective transcription factor DREB2A promotes thermotolerance of *Arabidopsis thaliana*. *J. Biol. Chem.* 294: 902–917.

Nakamichi, N., Kita, M., Ito, S., Yamashino, T. and Mizuno, T. (2005) PSEUDO-RESPONSE REGULATORS, PRR9, PRR7 and PRR5, together play essential roles close to the circadian clock of *Arabidopsis thaliana*. *Plant Cell Physiol.* 46: 686–698.

Nakamichi, N., Yamaguchi, J., Sato, A., Fujimoto, K.J. and Ota, E. (2022) Chemical biology to dissect molecular mechanisms underlying plant circadian clocks. *New Phytol.* 235: 1336–1343.

Nohales, M.A. and Kay, S.A. (2016) Molecular mechanisms at the core of the plant circadian oscillator. *Nat. Struct. Mol. Biol.* 23: 1061–1069.

Ono, A., Sato, A., Fujimoto, K.J., Matsuo, H., Yanai, T., Kinoshita, T., et al. (2019) 3,4-Dibromo-7-azaindole modulates Arabidopsis circadian clock by inhibiting casein kinase 1 activity. *Plant Cell Physiol.* 60: 2360–2368.

Poznanski, J., Poznanska, A. and Shugar, D. (2014) A Protein Data Bank survey reveals shortening of intermolecular hydrogen bonds in ligand-protein complexes when a halogenated ligand is an H-bond donor. *PLOS One* 9: e99984.

Saito, A.N., Matsuo, H., Kuwata, K., Ono, A., Kinoshita, T., Yamaguchi, J., et al. (2019) Structure-function study of a novel inhibitor of the casein kinase 1 family in *Arabidopsis thaliana*. *Plant Direct* 3: e00172.

R Core Team. (2022) R: A language and environment for statistical computing. R Foundation for Statistical Computing, Vienna, Austria.

Uehara, T.N., Mizutani, Y., Kuwata, K., Hirota, T., Sato, A., Mizoi, J., et al. (2019) Casein kinase 1 family regulates PRR5 and TOC1 in the Arabidopsis circadian clock. *Proc. Natl. Acad. Sci. U.S.A.* 116: 11528–11536.

Uehara, T.N., Nonoyama, T., Taki, K., Kuwata, K., Sato, A., Fujimoto, K.J., et al. (2022) Phosphorylation of RNA polymerase II by CDKC;2 maintains the Arabidopsis circadian clock period. *Plant Cell Physiol.* 63: 450–462.

Wang, Z.W., Wu, Z., Raitskin, O., Sun, Q. and Dean, C. (2014) Antisense-mediated FLC transcriptional repression requires the P-TEFb transcription elongation factor. *Proc. Natl. Acad. Sci. U.S.A.* 111: 7468–7473.

Webb, B. and Sali, A. (2016) Comparative protein structure modeling using modeller. *Curr. Protoc. Bioinformatics* 54: 5.6.1–5.6.37. *John Wiley & Sons, Inc.*

Yan, J.P., Kim, Y.J. and Somers, D.E. (2021) Post-translational mechanisms of plant circadian regulation. *Genes (Basel)* 12: genes12030325.